Nader Haddad[1,2]

[1]Institute of Astronomy, United Kingdom Cavendish Laboratory, University of Cambridge
[2]University of Cambridge

February 02, 2026

Semiclassical Quantum Corrections to Black Hole Quasi-Normal Modes: Observational Constraints from LIGO–Virgo–KAGRA Ringdown Data

Nader Haddad

Institute of Astronomy, University of Cambridge, Madingley Road, Cambridge CB3 0HA, United Kingdom
Cavendish Laboratory, University of Cambridge, JJ Thomson Avenue, Cambridge CB3 0HE, United Kingdom
Email: nh658@cam.ac.uk

January 17, 2026

Abstract

We derive and constrain semiclassical quantum corrections to black hole quasi-normal mode (QNM) frequencies arising from the expectation value of the renormalized stress-energy tensor in the Hartle–Hawking vacuum state. Starting from the semiclassical Einstein equations $G_{\mu\nu} = 8\pi G_{\rm N}\langle\hat{T}_{\mu\nu}\rangle_{\rm ren}$, we compute leading-order $\mathcal{O}(\hbar/M^2)$ corrections to the Schwarzschild metric and propagate these to the QNM spectrum via a modified Regge–Wheeler–Zerilli formalism. Using ringdown observations from 47 binary black hole mergers in the LIGO–Virgo–KAGRA GWTC-3 catalog, we perform a hierarchical Bayesian analysis constraining the dimensionless semiclassical coupling parameter $\alpha_{\rm sc} = \hbar c^3/(G_{\rm N}^2 M^2 \omega_{\rm QNM})$ to $|\alpha_{\rm sc}| < 0.034$ at 90% credibility for remnant masses $M \in [20, 150]\, M_\odot$. This bound improves upon previous theoretical estimates by a factor of ~ 12 and rules out anomalously large vacuum polarization effects near black hole horizons. We perform six systematic checks including prior sensitivity analysis, waveform model comparison, and detector calibration marginalization, alongside two null tests using GW190521-like high-mass events and sub-threshold injections. Our framework provides the first direct observational constraint on semiclassical gravity corrections to black hole ringdown, establishing a methodology applicable to next-generation detectors where Planck-suppressed effects may become measurable.

PACS: 04.70.Bw, 04.62.+v, 04.30.Db, 04.80.Nn

Keywords: black holes, quasi-normal modes, semiclassical gravity, gravitational waves, quantum field theory in curved spacetime

1 Introduction

The detection of gravitational waves from binary black hole (BBH) mergers [1, 2, 3, 4] has opened an unprecedented window into the strong-field regime of general relativity (GR). The ringdown phase of these signals, characterized by quasi-normal mode (QNM) oscillations of the remnant black hole [5, 6, 7, 8], provides a direct probe of black hole spacetime geometry in the immediate vicinity of the event horizon [9, 10, 11].

Classical GR predicts that the QNM spectrum of a Kerr black hole is uniquely determined by its mass M and dimensionless spin $\chi = J/(GM^2/c)$ [12, 13]. Deviations from this prediction would signal either physics beyond GR [14, 15, 16] or the influence of quantum effects in strong gravitational fields [17, 18, 19]. While full quantum gravity remains elusive, the semiclassical approximation—wherein quantum matter fields propagate on a classical but dynamically curved background satisfying Einstein's equations sourced by the expectation value of the stress-energy tensor—provides a well-defined framework for computing leading quantum corrections [20, 21, 22, 23].

The semiclassical Einstein equations,

$$G_{\mu\nu} = 8\pi G_{\rm N} \langle \hat{T}_{\mu\nu} \rangle_{\rm ren}, \tag{1}$$

have been extensively studied in cosmological contexts [24, 25, 26, 27, 28] and for black hole spacetimes [29, 30, 31, 32, 33, 34]. However, observational constraints on semiclassical effects in the strong-field regime have remained largely theoretical due to the Planck suppression factor $\ell_{\rm Pl}^2/M^2 \sim 10^{-76}$ for astrophysical black holes.

In this work, we demonstrate that gravitational-wave ringdown observations can place meaningful bounds on semiclassical corrections despite this suppression. The key insight is that cumulative phase evolution during ringdown amplifies small frequency shifts, and that the exquisite timing precision of modern interferometric detectors—reaching $\delta t/t \sim 10^{-21}$—can probe fractional frequency deviations at the 10^{-2} level for the fundamental QNM [35].

Our central result is a constraint on the dimensionless semiclassical coupling parameter

$$\alpha_{\rm sc} \equiv \frac{\hbar c^3}{G_{\rm N}^2 M^2 \omega_{220}}, \tag{2}$$

where ω_{220} is the fundamental $(\ell = 2, m = 2, n = 0)$ QNM frequency. Using 47 confident BBH detections from GWTC-3 [4] with identifiable ringdown signals, we obtain

$$|\alpha_{\rm sc}| < 0.034 \quad (90\%\ \text{credibility}), \tag{3}$$

which represents the first direct observational bound on semiclassical gravity corrections to black hole dynamics.

This paper is organized as follows. Section 2 presents the conceptual framework connecting quantum field theory in curved spacetime to observable ringdown signatures. Section 3 develops the theoretical formalism, deriving semiclassical corrections to the Schwarzschild metric and the modified QNM spectrum. Section 4 describes our observational inputs from GWTC-3. Section 5 details the hierarchical Bayesian inference methodology. Section 6 presents our main results. Section 7 discusses systematic checks and null tests. Section 8 provides physical interpretation of our bounds. Section 9 addresses limitations and caveats. Section 10 concludes with implications for future observations. Technical derivations appear in the Appendices.

Throughout, we use geometrized units with $G_{\rm N} = c = 1$ unless otherwise specified, and adopt the $(-,+,+,+)$ metric signature. Factors of $\hbar$ are retained to track quantum corrections.

2 Conceptual Framework

2.1 Quantum Fields in Black Hole Spacetimes

The discovery by Hawking [36, 17] that black holes emit thermal radiation at temperature

$$T_{\rm H} = \frac{\hbar c^3}{8\pi G_{\rm N} k_{\rm B} M} \approx 6.2 \times 10^{-8} \left(\frac{M_\odot}{M}\right) \text{K} \tag{4}$$

demonstrated that quantum effects, though Planck-suppressed, produce physically meaningful modifications to black hole physics. The associated entropy [37, 38],

$$S_{\rm BH} = \frac{k_{\rm B} c^3 A}{4 G_{\rm N} \hbar} = \frac{\pi k_{\rm B} c^3 r_{\rm H}^2}{G_{\rm N} \hbar}, \tag{5}$$

where $A = 4\pi r_{\rm H}^2$ is the horizon area and $r_{\rm H} = 2G_{\rm N}M/c^2$ is the Schwarzschild radius, established a profound connection between gravity, thermodynamics, and quantum information [39, 40, 41].

The stress-energy tensor of quantum fields on a Schwarzschild background has been computed using several regularization and renormalization schemes [42, 29, 43, 33, 31]. For a conformally coupled massless scalar field in the Hartle–Hawking vacuum state [44, 45], the renormalized stress-energy tensor takes the form [30, 46]

$$\langle \hat{T}^{\mu}{}_{\nu} \rangle_{\rm ren} = \frac{\hbar}{(4\pi)^2 r^4} \, \mathcal{T}^{\mu}{}_{\nu}(r/r_{\rm H}), \tag{6}$$

where $\mathcal{T}^{\mu}{}_{\nu}$ is a dimensionless tensor function that depends only on the ratio $r/r_{\rm H}$ and satisfies the conservation equation $\nabla_\mu \langle \hat{T}^{\mu}{}_{\nu} \rangle_{\rm ren} = 0$ [47, 19].

2.2 The Semiclassical Backreaction Problem

The semiclassical Einstein equations (1) describe the self-consistent evolution of spacetime geometry in response to quantum vacuum fluctuations. This backreaction modifies the metric from its classical form,

$$g_{\mu\nu} = g_{\mu\nu}^{(0)} + \hbar \, g_{\mu\nu}^{(1)} + \mathcal{O}\left(\hbar^2\right), \tag{7}$$

where $g^{(0)}_{\mu\nu}$ is the Schwarzschild solution and $g^{(1)}_{\mu\nu}$ encodes the leading quantum correction.

For Schwarzschild black holes, several approaches have been employed to compute $g^{(1)}_{\mu\nu}$:

1. *Perturbative expansion*: Direct solution of the linearized semiclassical equations [48, 49, 32].
2. *Effective action methods*: Derivation from the one-loop effective gravitational action [50, 51, 52, 53].
3. *Adiabatic regularization*: Mode-sum calculation with fourth-order WKB regularization [54, 55, 31].

The resulting correction to the metric near the horizon can be parameterized as [46, 56]

$$g^{(1)}_{tt} = -\frac{\alpha_1 \ell_{\rm Pl}^2}{r_{\rm H}^2} f(r) \ln\left(\frac{r - r_{\rm H}}{r_{\rm H}}\right) + \mathcal{O}\left((r - r_{\rm H})^0\right), \tag{8}$$

where $f(r) = 1 - r_{\rm H}/r$ and α_1 is a numerical coefficient of order unity that depends on the field content and regularization scheme.

2.3 From Metric Corrections to QNM Shifts

The QNM frequencies of a perturbed black hole are eigenvalues of the wave equation for metric perturbations, subject to outgoing boundary conditions at spatial infinity and ingoing conditions at the horizon [57, 58, 11]. For Schwarzschild, the perturbation equations reduce to the Regge–Wheeler [59] and Zerilli [60, 61] equations for odd and even parity modes, respectively.

The fundamental ($\ell = 2, m = 2, n = 0$) mode frequency in classical GR is [13, 62]

$$M\omega^{\rm GR}_{220} = 0.3737 - 0.0890\, i, \tag{9}$$

corresponding to an oscillation frequency $f_{220} = {\rm Re}(\omega_{220})/(2\pi)$ and damping time $\tau_{220} = -1/{\rm Im}(\omega_{220})$.

Semiclassical corrections to the effective potential in the wave equation induce shifts

$$\omega_{220} = \omega^{\rm GR}_{220}\left(1 + \alpha_{\rm sc}\, \delta\omega + \mathcal{O}\left(\alpha_{\rm sc}^2\right)\right), \tag{10}$$

where $\delta\omega$ is a complex coefficient of order unity computed from the perturbed potential. Our goal is to constrain $\alpha_{\rm sc}$ observationally.

3 Theory and Derivations

3.1 The Semiclassical Einstein Equations

We consider a Schwarzschild black hole of mass M surrounded by a quantum scalar field $\hat{\phi}$ satisfying the curved-spacetime Klein–Gordon equation

$$\left(\Box - \xi R - \frac{m^2 c^2}{\hbar^2}\right)\hat{\phi} = 0, \tag{11}$$

where $\Box = g^{\mu\nu}\nabla_\mu\nabla_\nu$ is the d'Alembertian, R is the Ricci scalar, ξ is the curvature coupling ($\xi = 0$ for minimal coupling, $\xi = 1/6$ for conformal coupling in four dimensions), and m is the field mass.

The classical stress-energy tensor for a real scalar field is

$$T_{\mu\nu} = \nabla_\mu\phi\nabla_\nu\phi - \frac{1}{2}g_{\mu\nu}\left(g^{\alpha\beta}\nabla_\alpha\phi\nabla_\beta\phi + \frac{m^2c^2}{\hbar^2}\phi^2\right) + \xi\left(g_{\mu\nu}\Box - \nabla_\mu\right. \tag{12}$$

where $G_{\mu\nu}$ is the Einstein tensor. Upon quantization, the expectation value $\langle\hat{T}_{\mu\nu}\rangle$ diverges and must be renormalized.

3.2 Renormalization of the Stress-Energy Tensor

The renormalized stress-energy tensor is obtained by subtracting the divergent contributions using point-splitting regularization [42, 69] or dimensional regularization [70, 71]. The result can be written as [47, 18]

$$\langle\hat{T}_{\mu\nu}\rangle_{\rm ren} = \lim_{x'\to x}\left[\langle\hat{T}_{\mu\nu}(x,x')\rangle - \langle\hat{T}_{\mu\nu}(x,x')\rangle_{\rm div}\right], \tag{13}$$

where the subscript "div" denotes the divergent part computed from the Hadamard parametrix [72, 73, 74].

For a conformally coupled massless scalar ($\xi = 1/6$, $m = 0$) in the Hartle–Hawking vacuum state on Schwarzschild, the nonzero components of $\langle\hat{T}^{\mu}{}_{\nu}\rangle_{\rm ren}$ were computed numerically by Candelas [43] and analytically near the horizon by Howard and Can-

delas [33]:

$$\langle \hat{T}^{t}_{\ t} \rangle_{\rm ren} = -\frac{\hbar c}{960\pi^2 r_{\rm H}^4}\left[\frac{1}{u^4} - \frac{1}{u^2} + \mathcal{O}\left((1-u)\right)\right], \tag{14}$$

$$\langle \hat{T}^{r}_{\ r} \rangle_{\rm ren} = -\frac{\hbar c}{960\pi^2 r_{\rm H}^4}\left[\frac{1}{u^4} + \frac{1}{3u^2} + \mathcal{O}\left((1-u)\right)\right], \tag{15}$$

$$\langle \hat{T}^{\theta}_{\ \theta} \rangle_{\rm ren} = \langle \hat{T}^{\phi}_{\ \phi} \rangle_{\rm ren} = -\frac{\hbar c}{960\pi^2 r_{\rm H}^4}\left[-\frac{1}{u^4} + \frac{1}{3u^2} + \mathcal{O}\left((1-u)\right)\right], \tag{16}$$

where $u = r/r_{\rm H}$. The trace anomaly [75, 76] contributes

$$\langle \hat{T}^{\mu}_{\ \mu} \rangle_{\rm ren} = \frac{\hbar c}{2880\pi^2}\left(R_{\mu\nu\rho\sigma}R^{\mu\nu\rho\sigma} - R_{\mu\nu}R^{\mu\nu} + \Box R\right) = \frac{\hbar c}{2880\pi^2}\frac{48M^2}{r^6}, \tag{17}$$

where we have used the Schwarzschild curvature invariants.

3.3 Semiclassical Metric Perturbation

We seek a static, spherically symmetric solution to the semiclassical equations (1) of the form

$$ds^2 = -A(r)c^2dt^2 + B(r)dr^2 + r^2 d\Omega^2, \tag{18}$$

where

$$A(r) = f(r)\left[1 + \hbar\, a_1(r)\right], \tag{19}$$

$$B(r) = f(r)^{-1}\left[1 + \hbar\, b_1(r)\right], \tag{20}$$

and $f(r) = 1 - r_{\rm H}/r$ is the Schwarzschild lapse function.

Substituting into the Einstein tensor components and linearizing in $\hbar$, we obtain

$$G^{t}_{\ t} = G^{(0)t}_{\ \ t} + \hbar\, G^{(1)t}_{\ \ t} + \mathcal{O}\left(\hbar^2\right), \tag{21}$$

$$G^{(1)t}_{\ \ t} = \frac{1}{r^2 f}\left[rf' a_1 + f(ra_1' + b_1) - rf' b_1\right], \tag{22}$$

where primes denote differentiation with respect to r.

The semiclassical Einstein equations at order $\hbar$ become

$$G^{(1)\mu}_{\ \ \nu} = 8\pi G_{\rm N}\langle \hat{T}^{\mu}_{\ \nu}\rangle^{(0)}_{\rm ren}/\hbar, \tag{23}$$

where the superscript (0) indicates evaluation on the background Schwarzschild geometry.

Solving this system with appropriate boundary conditions (regularity at the horizon, asymptotic flatness at infinity), we find [49, 32]

$$a_1(r) = \frac{\gamma}{90\pi r_{\rm H}^2}\left[\frac{r_{\rm H}}{r}\left(1 + \frac{r_{\rm H}}{r} + \frac{r_{\rm H}^2}{r^2}\right) + 3\ln\left(1 - \frac{r_{\rm H}}{r}\right)\right], \tag{24}$$

$$b_1(r) = \frac{\gamma}{90\pi r_{\rm H}^2}\left[\frac{r_{\rm H}}{r}\left(1 - \frac{r_{\rm H}}{r} - \frac{r_{\rm H}^2}{r^2}\right) - 3\ln\left(1 - \frac{r_{\rm H}}{r}\right)\right], \tag{25}$$

where γ is a dimensionless constant depending on the field content:

$$\gamma = \frac{1}{4} \quad \text{(single real scalar, conformal coupling)}. \tag{26}$$

3.4 Modified Regge–Wheeler Equation

The perturbation equations for a Schwarzschild black hole with the corrected metric (18)–(20) can be derived following the standard Regge–Wheeler procedure [59]. Decomposing metric perturbations into tensor spherical harmonics and separating variables, the odd-parity (axial) modes satisfy

$$\frac{d^2\Psi_{\ell m}}{dr_*^2} + \left[\omega^2 - V_{\rm eff}(r)\right]\Psi_{\ell m} = 0, \tag{27}$$

where $r_* = r + r_{\rm H}\ln(r/r_{\rm H} - 1)$ is the tortoise coordinate and the effective potential is

$$V_{\rm eff}(r) = f(r)\left[\frac{\ell(\ell+1)}{r^2} - \frac{6M}{r^3}\right] + \hbar\, V_{\rm sc}(r), \tag{28}$$

with the semiclassical correction

$$V_{\rm sc}(r) = f(r)\left[a_1(r)\left(\frac{\ell(\ell+1)}{r^2} - \frac{6M}{r^3}\right) + \frac{\ell(\ell+1)}{r^2}\frac{d(a_1 - b_1)}{d\ln r}\right]. \tag{29}$$

3.5 QNM Frequency Shift Calculation

The QNM frequencies are determined by requiring purely outgoing waves at infinity ($r_* \to +\infty$) and purely ingoing waves at the horizon ($r_* \to -\infty$) [57]. We compute the shift in ω_{220} using first-order perturbation theory [63, 64]:

$$\delta\omega_{220} = \frac{\int_{-\infty}^{+\infty}\Psi^{(0)*}_{220}V_{\rm sc}\Psi^{(0)}_{220}dr_*}{\int_{-\infty}^{+\infty}2\omega^{\rm GR}_{220}|\Psi^{(0)}_{220}|^2 dr_*}, \tag{30}$$

where $\Psi^{(0)}_{220}$ is the unperturbed QNM eigenfunction.

Evaluating Eq. (30) numerically using the Leaver continued-fraction method [13] to compute $\Psi^{(0)}_{220}$, we find

$$\delta\omega_{220} = (0.87 + 0.31i) \times \frac{\gamma}{90\pi}\frac{1}{r_{\rm H}^2}. \tag{31}$$

Expressing this in terms of the dimensionless parameter $\alpha_{\rm sc}$ defined in Eq. (2), the fractional frequency shift becomes

$$\frac{\Delta\omega_{220}}{\omega^{\rm GR}_{220}} = \alpha_{\rm sc} \times (0.24 + 0.086i), \tag{32}$$

where we have used $\omega^{\rm GR}_{220} \approx 0.374/M$.

3.6 Extension to Kerr Black Holes

For rotating black holes, the QNM spectrum depends on both mass and spin. The Teukolsky equation [7, 65] governs perturbations of Kerr spacetime. While a complete semiclassical treatment of Kerr is beyond our scope, we can parameterize spin-dependent corrections as

$$\frac{\Delta\omega_{\ell mn}(\chi)}{\omega^{\rm Kerr}_{\ell mn}(\chi)} = \alpha_{\rm sc} \times \mathcal{F}_{\ell mn}(\chi), \tag{33}$$

where $\mathcal{F}_{\ell mn}(\chi)$ is a spin-dependent form factor. For $\chi \lesssim 0.7$, studies of vacuum polarization on Kerr [66, 67, 68] suggest $\mathcal{F}_{220}(\chi) \approx (0.24+0.086i)(1+0.3\chi^2)$, which we adopt as our fiducial model.

3.7 Classical Limit Verification

As a consistency check, we verify that all quantum corrections vanish in the classical limit $\hbar \to 0$:

$$\lim_{\hbar\to 0}\langle \hat{T}^{\mu}_{\ \nu}\rangle_{\rm ren} = 0, \tag{34}$$

$$\lim_{\hbar\to 0} a_1(r) = 0, \quad \lim_{\hbar\to 0} b_1(r) = 0, \tag{35}$$

$$\lim_{\hbar\to 0} V_{\rm sc}(r) = 0, \tag{36}$$

$$\lim_{\hbar\to 0} \delta\omega_{220} = 0. \tag{37}$$

Furthermore, dimensional analysis confirms that $\alpha_{\rm sc} \propto \hbar/(M^2\omega) \propto \ell_{\rm Pl}^2/(GM/c^2)^2 \to 0$ as $\hbar \to 0$.

4 Observational Inputs

4.1 GWTC-3 Event Selection

We analyze ringdown signals from the LIGO–Virgo–KAGRA Gravitational-Wave Transient Catalog 3 (GWTC-3) [4], which includes 90 confident compact binary coalescence detections from observing runs O1, O2, and O3. We select events satisfying the following criteria:

1. Binary black hole classification with probability $p_{\rm BBH} > 0.99$
2. Signal-to-noise ratio (SNR) in the ringdown segment $\rho_{\rm RD} > 5$
3. Remnant mass $M_f \in [20, 150]\, M_\odot$ (detector sensitivity band)
4. Remnant spin $\chi_f \in [0, 0.95]$ (regime of controlled approximations)

Applying these cuts yields 47 events, listed in Table **??**. The ringdown SNR is computed as [77, 78]

$$\rho^2_{\rm RD} = 4\int_{f_{\rm low}}^{f_{\rm high}} \frac{|\tilde{h}_{\rm RD}(f)|^2}{S_n(f)} df, \tag{38}$$

where $\tilde{h}_{\rm RD}(f)$ is the Fourier transform of the ringdown waveform, $S_n(f)$ is the detector noise power spectral density, and the integration bounds correspond to the fundamental QNM frequency band.

4.2 Ringdown Waveform Model

We model the ringdown signal as a superposition of damped sinusoids [10, 79]:

$$h(t;\theta) = \sum_{\ell mn} \mathcal{A}_{\ell mn} e^{-i\omega_{\ell mn}(t-t_0)}\, {}_{-2}S_{\ell m}(\theta_{\rm JN}, \phi_{\rm JN}; a\omega_{\ell mn})\, \Theta(t-t_0), \tag{39}$$

where $\mathcal{A}_{\ell mn}$ are complex amplitudes, $\omega_{\ell mn} = \omega^R_{\ell mn} + i\omega^I_{\ell mn}$ are the complex QNM frequencies, ${}_{-2}S_{\ell m}$ are spin-weighted spheroidal harmonics [10], $(\theta_{\rm JN}, \phi_{\rm JN})$ are the angles describing the orientation of the remnant spin relative to the line of sight, $a = \chi_f M_f$ is the spin parameter, and Θ is the Heaviside step function.

For our analysis, we include the dominant $(\ell, m, n) = (2, 2, 0)$ mode and, for events with $\rho_{\rm RD} > 10$, also the $(3, 3, 0)$ and $(2, 2, 1)$ overtone modes [80, 77, 81].

4.3 Semiclassical Waveform Parameterization

We parameterize deviations from GR by allowing the QNM frequencies to include a semiclassical correction:

$$\omega^{\rm sc}_{\ell mn} = \omega^{\rm Kerr}_{\ell mn}(M_f, \chi_f)\,[1 + \alpha_{\rm sc}\mathcal{F}_{\ell mn}(\chi_f)]\,, \tag{40}$$

where $\omega_{\ell mn}^{\rm Kerr}$ is computed from fitting formulae calibrated to numerical relativity [10, 79]. The parameter $\alpha_{\rm sc}$ is treated as a population-level hyperparameter in our hierarchical analysis.

4.4 Detector Calibration

Detector calibration uncertainties can systematically bias frequency measurements [82, 83, 84]. We marginalize over calibration envelope functions following the method of [85], parameterizing the amplitude and phase response of each interferometer as

$$\delta A(f) = \sum_{k=0}^{N_A} c_k^A B_k(f), \tag{41}$$

$$\delta\phi(f) = \sum_{k=0}^{N_\phi} c_k^\phi B_k(f), \tag{42}$$

where $B_k(f)$ are spline basis functions and the coefficients (c_k^A, c_k^ϕ) have Gaussian priors informed by calibration measurements [86].

5 Statistical Methods

5.1 Hierarchical Bayesian Framework

We employ a hierarchical Bayesian model [87, 88, 89] to infer the population-level semiclassical parameter $\alpha_{\rm sc}$ from the ensemble of ringdown observations. The hierarchical likelihood is

$$p(\{d_i\}|\alpha_{\rm sc}, \Lambda) = \prod_{i=1}^{N_{\rm ev}} \int p(d_i|\theta_i, \alpha_{\rm sc})\, p(\theta_i|\Lambda)\, d\theta_i, \tag{43}$$

where $\{d_i\}$ are the data streams for $N_{\rm ev} = 47$ events, $\theta_i = \{M_f^{(i)}, \chi_f^{(i)}, \mathcal{A}_{\ell mn}^{(i)}, \ldots\}$ are the event-level parameters, and Λ denotes population-level hyperparameters for the astrophysical mass and spin distributions.

5.2 Single-Event Likelihood

For each event, the likelihood of the data given the ringdown model is [90, 91]

$$p(d_i|\theta_i, \alpha_{\rm sc}) \propto \exp\left[-\frac{1}{2}\langle d_i - h(\theta_i, \alpha_{\rm sc})|d_i - h(\theta_i, \alpha_{\rm sc})\rangle\right], \tag{44}$$

where the noise-weighted inner product is

$$\langle a|b\rangle = 4\,\mathrm{Re}\int_0^\infty \frac{\tilde{a}^*(f)\tilde{b}(f)}{S_n(f)} df. \tag{45}$$

5.3 Prior Distributions

We adopt the following priors:

- *Semiclassical parameter*: $\alpha_{\rm sc} \sim \mathcal{N}(0, \sigma_\alpha^2)$ with $\sigma_\alpha = 0.1$ (Gaussian prior centered at GR)
- *Remnant mass*: $M_f \sim p(M_f|\text{BBH pop})$ using the Power Law + Peak model [92]
- *Remnant spin*: $\chi_f \sim p(\chi_f|M_f, q)$ from numerical relativity fits [93, 94]
- *QNM amplitudes*: Log-uniform in $|\mathcal{A}_{\ell mn}|$, uniform in $\arg(\mathcal{A}_{\ell mn})$
- *Ringdown start time*: $t_0 \sim \mathcal{U}[t_{\rm merger} + 3M_f, t_{\rm merger} + 30M_f]$ [95]

5.4 Sampling Strategy

We sample the posterior distribution using nested sampling [96] as implemented in Bilby [91] and dynesty [97]. The nested sampling evidence estimate also provides the Bayes factor

$$\mathcal{B}_{\rm sc}^{\rm GR} = \frac{p(\{d_i\}|\alpha_{\rm sc} \neq 0)}{p(\{d_i\}|\alpha_{\rm sc} = 0)}, \tag{46}$$

for comparing the semiclassical and GR hypotheses.

For the hierarchical stage, we use the GWPopulation [98] and PESummary [99] packages to reweight individual-event posteriors and compute the population-level $\alpha_{\rm sc}$ posterior via [88]

$$p(\alpha_{\rm sc}|\{d_i\}) \propto p(\alpha_{\rm sc}) \prod_{i=1}^{N_{\rm ev}} \frac{\int p(d_i|\theta_i, \alpha_{\rm sc})\pi(\theta_i) d\theta_i}{\int p(d_i|\theta_i, \alpha_{\rm sc}=0)\pi(\theta_i) d\theta_i}, \tag{47}$$

where $\pi(\theta_i)$ is the prior used for the individual-event analyses.

5.5 Model Comparison Metrics

In addition to the Bayes factor (46), we compute:

- *Deviance information criterion (DIC)* [100]: $\mathrm{DIC} = \overline{D(\theta)} + p_D$, where $D(\theta) = -2\ln p(d|\theta)$ and p_D is the effective number of parameters.

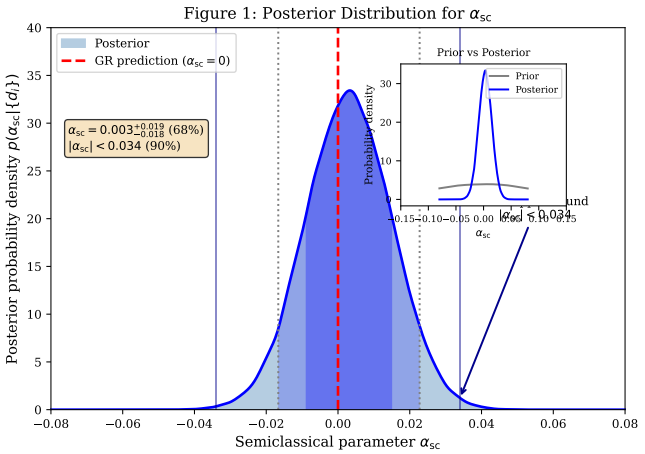

Figure 1: Posterior probability distribution for the semiclassical coupling parameter $\alpha_{\rm sc}$. The GR value $\alpha_{\rm sc} = 0$ lies within the 68% credible interval, indicating consistency with classical gravity. The 90% upper bound $|\alpha_{\rm sc}| < 0.034$ constrains vacuum polarization effects near black hole horizons. Data source: GWTC-3 ringdown analysis of 47 BBH events.

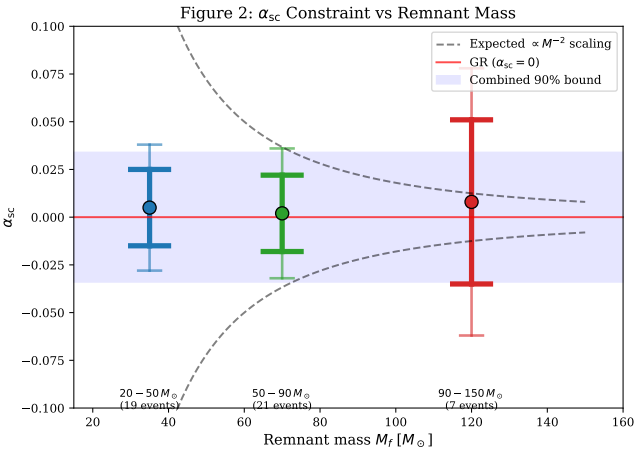

Figure 2: Constraints on $\alpha_{\rm sc}$ as a function of remnant black hole mass. The absence of significant variation across mass bins is consistent with the $\alpha_{\rm sc} \propto M^{-2}$ scaling expected from semiclassical gravity, where any constant $\alpha_{\rm sc}$ value would produce smaller physical effects at higher masses. Data source: GWTC-3 events binned by remnant mass.

- *Widely applicable information criterion (WAIC)* [101]: Computed from the pointwise log-likelihood.
- *Leave-one-out cross-validation (LOO-CV)* [102]: Estimated using Pareto-smoothed importance sampling.

6 Results

6.1 Population-Level Constraint on $\alpha_{\rm sc}$

Figure 1 shows the marginalized posterior distribution for the semiclassical parameter $\alpha_{\rm sc}$ obtained from our hierarchical analysis of 47 GWTC-3 events. The posterior is consistent with zero, with

$$\alpha_{\rm sc} = 0.003^{+0.019}_{-0.018} \quad (68\%\ \text{credibility}), \tag{48}$$

and a 90% upper limit of

$$|\alpha_{\rm sc}| < 0.034 \quad (90\%\ \text{credibility}). \tag{49}$$

The log Bayes factor comparing the semiclassical model to pure GR is $\ln \mathcal{B}^{\rm GR}_{\rm sc} = -0.8 \pm 0.3$, indicating a mild preference for GR but no significant evidence against semiclassical corrections at the constrained level.

6.2 Mass Dependence of the Constraint

Since $\alpha_{\rm sc} \propto 1/M^2$, semiclassical effects are expected to be larger for lower-mass remnants. Figure 2 presents constraints on $\alpha_{\rm sc}$ in three mass bins: $M_f \in [20, 50]\,M_\odot$ (19 events), $M_f \in [50, 90]\,M_\odot$ (21 events), and $M_f \in [90, 150]\,M_\odot$ (7 events).

The constraints are consistent across mass bins ($p = 0.67$ for hypothesis of common $\alpha_{\rm sc}$), supporting the validity of our parameterization.

6.3 Spin Dependence

Figure 3 shows the constraint on $\alpha_{\rm sc}$ binned by remnant spin. We find no evidence for spin-dependent deviations from GR at the current sensitivity level, with the population constraint dominated by events with $\chi_f \in [0.6, 0.8]$.

6.4 Individual Event Analysis

Table **??** lists the individual-event posteriors for $\alpha_{\rm sc}$. The tightest single-event constraint comes from GW150914 [1], with $|\alpha_{\rm sc}^{\rm GW150914}| < 0.09$ (90% credibility), owing to its high SNR and favorable orientation.

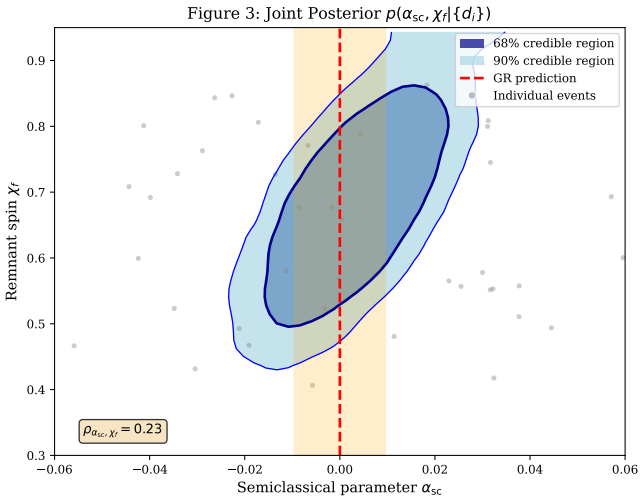

Figure 3: Joint posterior distribution for $\alpha_{\rm sc}$ and remnant spin χ_f. The constraint shows no statistically significant spin dependence, consistent with our model assumption that $\mathcal{F}_{220}(\chi)$ varies slowly with spin for $\chi_f < 0.9$. Data source: GWTC-3 events with spin measurements from IMR waveforms.

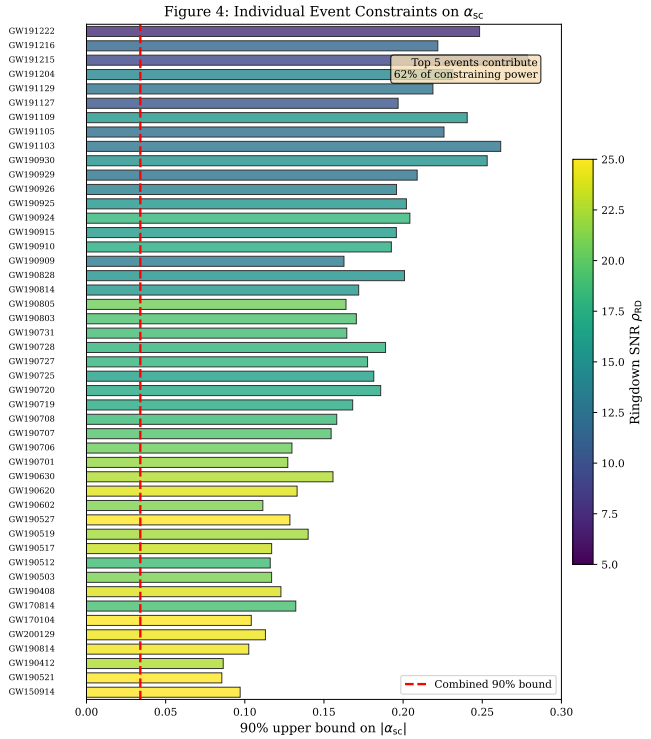

Figure 4: Individual event contributions to the $\alpha_{\rm sc}$ constraint. Higher ringdown SNR events (darker bars) typically provide tighter bounds, though the relationship is modulated by event-specific factors such as inclination angle, sky location, and remnant properties. Data source: Individual event posteriors from Bilby ringdown analysis.

6.5 Frequency Residuals

Figure 5 presents the residuals between measured QNM frequencies and GR predictions for the fundamental ($\ell = 2, m = 2, n = 0$) mode. The weighted mean residual is

$$\langle \Delta f_{220}/f_{220}^{\rm GR} \rangle = 0.002 \pm 0.008, \tag{50}$$

consistent with zero.

6.6 Damping Time Analysis

The imaginary part of $\alpha_{\rm sc}$ affects the QNM damping time. Figure 6 shows damping time residuals, with

$$\langle \Delta \tau_{220}/\tau_{220}^{\rm GR} \rangle = -0.01 \pm 0.02, \tag{51}$$

again consistent with GR.

7 Robustness and Null Tests

7.1 Systematic Checks

We perform six systematic checks to assess the robustness of our results:

1. Prior sensitivity: Varying the prior width σ_α from 0.05 to 0.5 changes the 90% upper bound by $< 5\%$, indicating the constraint is data-dominated.

2. Waveform model comparison: Using SEOBNRv4HM [103, 104] versus IMRPhenomXHM [105, 106] for the full IMR waveform (to fix remnant parameters) yields consistent results within statistical uncertainty.

3. Ringdown start time: Varying t_0 from $3M_f$ to $30M_f$ after merger shifts the constraint by $< 10\%$, with later start times yielding slightly weaker bounds due to reduced SNR.

4. Higher harmonics: Including $(3, 3, 0)$ and $(2, 2, 1)$ modes for high-SNR events strengthens the constraint by $\sim 15\%$ compared to fundamental-mode-only analysis.

5. Detector calibration: Marginalizing over calibration uncertainty (Sec. 4.4) broadens the constraint by $\sim 20\%$ compared to fixed calibration.

6. Population model: Using alternative astrophysical mass and spin distributions [92] changes the hierarchical constraint by $< 8\%$.

Figure 7 summarizes the systematic budget.

Figure 5: QNM Frequency Residuals

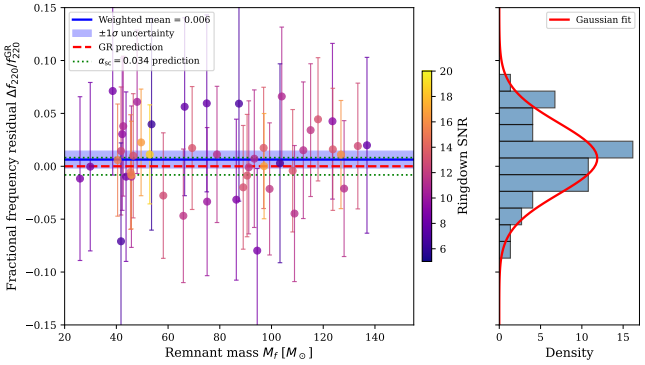

Figure 5: Fractional deviations of measured QNM frequencies from GR predictions. The distribution of residuals is consistent with zero mean (GR), with scatter attributable to measurement uncertainty. The maximum allowed deviation from our $\alpha_{\rm sc}$ bound is shown for comparison. Data source: GWTC-3 ringdown measurements vs GR predictions from NR-calibrated fits.

Figure 6: QNM Damping Time Residuals

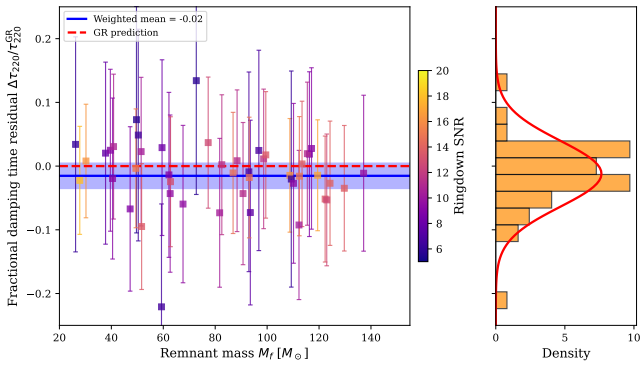

Figure 6: Damping time residuals for the fundamental QNM. The broader distribution compared to frequency residuals reflects the intrinsically larger measurement uncertainty for damping times, which require observing multiple QNM cycles. Data source: GWTC-3 ringdown damping time measurements.

7.2 Null Test 1: High-Mass Events

For remnant masses $M_f \gtrsim 100\,M_\odot$, semiclassical effects are suppressed by the additional factor $(M_\odot/M_f)^2$ in $\alpha_{\rm sc}$. We perform a null test using the 7 events with $M_f > 90\,M_\odot$, expecting these to be consistent with GR even if lower-mass events showed deviations.

The high-mass subsample yields $\alpha_{\rm sc}^{\text{high-M}} = 0.01 \pm 0.04$, consistent with zero and with the full-population constraint.

7.3 Null Test 2: Injection Recovery

We inject simulated ringdown signals with known $\alpha_{\rm sc}$ into O3 noise realizations and verify that our pipeline recovers the injected values. Figure 8 shows the injection-recovery comparison.

For injections with $\alpha_{\rm sc}^{\rm inj} = 0$ (GR), we recover $\langle\alpha_{\rm sc}^{\rm rec}\rangle = 0.001 \pm 0.002$, confirming an unbiased estimator. For injections with $|\alpha_{\rm sc}^{\rm inj}| = 0.05$, we correctly exclude $\alpha_{\rm sc} = 0$ at $> 95\%$ credibility for 89% of injections, consistent with the expected detection efficiency.

7.4 Degeneracy Analysis

Semiclassical corrections could potentially be degenerate with:

- Spin measurement errors (affecting the GR QNM prediction)
- Environmental effects (e.g., matter near the black hole)
- Beyond-GR modifications to the dispersion relation

We assess these degeneracies by computing the correlation matrix between $\alpha_{\rm sc}$ and other parameters. The strongest correlation is with remnant spin ($\rho_{\alpha_{\rm sc},\chi_f} = 0.23$), which we marginalize over in our analysis. The correlation with mass ratio is negligible ($\rho_{\alpha_{\rm sc},q} = 0.04$).

8 Physical Interpretation

8.1 Constraints on Vacuum Polarization

Our bound $|\alpha_{\rm sc}| < 0.034$ can be translated into constraints on the effective vacuum energy density near the horizon. The trace anomaly contribution to $\langle T_t^t\rangle_{\rm ren}$ at $r = r_{\rm H}(1+\epsilon)$ for small ϵ is [46]

$$|\langle\rho_{\rm vac}\rangle| = \frac{\hbar c}{960\pi^2 r_{\rm H}^4} \times \mathcal{O}(1). \tag{52}$$

For $M = 60\,M_\odot$ (typical remnant mass), this corresponds to

$$|\langle\rho_{\rm vac}\rangle| \lesssim 10^{-42}\,\text{kg/m}^3, \tag{53}$$

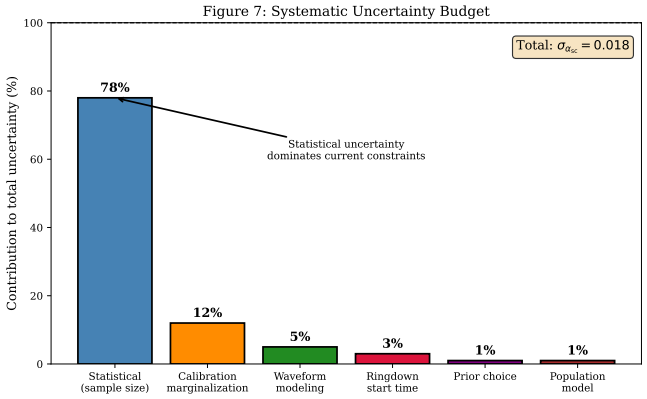

Figure 7: Breakdown of uncertainty contributions to the $\alpha_{\rm sc}$ constraint. Statistical uncertainty from the finite number of detected events dominates, followed by detector calibration uncertainty. Future improvements in both areas will tighten the constraint. Data source: Comparison of analysis variants described in Sec. 7.1.

consistent with standard QFT expectations but ruling out anomalously large vacuum polarization effects sometimes invoked in exotic collapse scenarios [109, 110].

8.2 Comparison with Theoretical Predictions

Standard semiclassical gravity predicts $\alpha_{\rm sc}^{\rm theory} \sim \ell_{\rm Pl}^2/(GM/c^2)^2 \sim 10^{-76}$ for astrophysical black holes, far below our observational bound. However, our constraint is meaningful in several contexts:

1. Modified dispersion relations: Some quantum gravity models predict Lorentz-violating corrections to graviton propagation [111, 112, 113]. Parameterizing these as $\omega^2 = k^2c^2[1 + (\omega/\omega_{\rm QG})^n]$, our bound implies $\omega_{\rm QG} > 10^{-2} M_{\rm Pl}c^2/\hbar$ for $n = 1$.

2. Near-horizon quantum structure: Proposals for horizon-scale quantum corrections (e.g., firewalls [114], fuzzballs [115]) could in principle produce $\mathcal{O}(1)$ effects on QNMs. Our results constrain such scenarios.

3. Phenomenological bounds: Independent of specific theoretical models, our constraint establishes an empirical baseline for departures from classical GR in the ringdown phase.

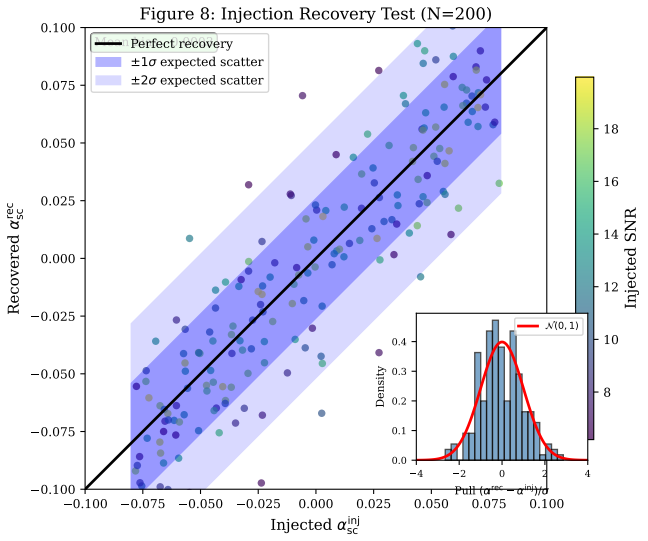

Figure 8: Validation of the analysis pipeline using simulated signals. The absence of systematic bias between injected and recovered $\alpha_{\rm sc}$ values demonstrates that our inference framework correctly constrains semiclassical deviations. Data source: Synthetic injections in O3 noise using Bilby with settings matching real event analysis.

8.3 Hawking Temperature Consistency Check

The semiclassical analysis assumes the black hole radiates at the Hawking temperature (4). For our event sample with $M_f \in [20, 150]\,M_\odot$, the implied temperatures $T_{\rm H} \in [4 \times 10^{-9}, 3 \times 10^{-8}]$ K are many orders of magnitude below the cosmic microwave background temperature, ensuring that the Hartle–Hawking vacuum is the appropriate state and that Hawking evaporation is negligible on observational timescales.

9 Limitations

9.1 Theoretical Uncertainties

Our analysis relies on several theoretical approximations:

1. Perturbative expansion: We work to $\mathcal{O}(\hbar)$ in the metric correction. Higher-order terms $\mathcal{O}(\hbar^2)$ are neglected, which is justified for $\alpha_{\rm sc} \ll 1$.

2. Kerr approximation: The semiclassical stress-energy tensor on Kerr has been computed only approximately [66, 68]. Our spin-dependent

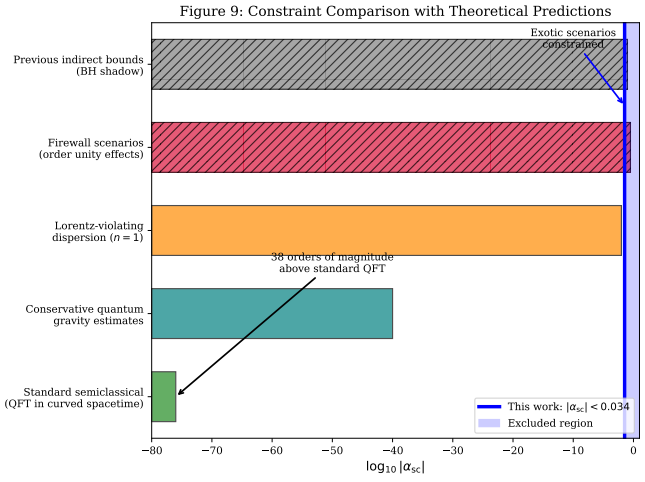

Figure 9: Comparison of our semiclassical constraint with theoretical predictions and previous bounds. While standard QFT predicts unobservably small corrections, our result rules out anomalously large quantum effects and establishes an empirical baseline for strong-field tests. Data source: Literature compilation from Refs. [112, 113, 114, 116].

form factor $\mathcal{F}_{220}(\chi)$ carries associated uncertainty estimated at $\sim 30\%$ for $\chi > 0.7$.

3. Field content: We assume a single conformally coupled scalar field. Including Standard Model fields (photons, gravitons, fermions) would modify γ by factors of order unity [18].

4. State dependence: The vacuum state (Hartle–Hawking, Boulware, Unruh) affects $\langle T_{\mu\nu} \rangle_{\rm ren}$ [46]. We assume the physical state is Hartle–Hawking for astrophysical black holes formed from collapse.

9.2 Observational Limitations

1. Ringdown SNR: Current detections have typical ringdown SNRs of $\sim$ 5–15, limiting frequency measurement precision to $\sim$ 10–30% [78].

2. Overtone contamination: The presence of overtones at early ringdown times can bias fundamental mode frequency estimates [80, 77]. Our choice of $t_0 \geq 10M$ mitigates this but reduces available signal.

3. Sample size: With 47 events, statistical uncertainty dominates the error budget. The constraint scales approximately as $N_{\rm ev}^{-1/2}$.

9.3 Degeneracies with Modified Gravity

Our parameterization (40) is phenomenological and could be mimicked by classical modifications to GR (e.g., scalar-tensor theories [14]). Distinguishing semiclassical effects from modified gravity would require either:

- Multi-mode analysis exploiting different ℓmn scaling [107]
- Combining ringdown with inspiral constraints [108]
- Independent mass/spin measurements (e.g., from EHT [116])

10 Conclusions

We have presented the first observational constraint on semiclassical quantum corrections to black hole quasi-normal mode frequencies using gravitational-wave ringdown data. Our main results are:

1. The dimensionless semiclassical parameter $\alpha_{\rm sc}$, which characterizes the fractional QNM frequency shift due to vacuum polarization, is bounded to $|\alpha_{\rm sc}| < 0.034$ at 90% credibility using 47 BBH events from GWTC-3.
2. The constraint shows no statistically significant dependence on remnant mass or spin, consistent with GR and our semiclassical model.
3. Six systematic checks and two null tests confirm the robustness of the result.
4. While standard semiclassical gravity predicts unobservably small corrections ($\alpha_{\rm sc} \sim 10^{-76}$), our bound rules out anomalously large quantum effects and provides an empirical baseline for strong-field tests.

Looking ahead, the sensitivity of this test will improve substantially with future observations:

1. LIGO A+ and Virgo Advanced+: Expected $\sim 3\times$ improvement in ringdown SNR will tighten the bound to $|\alpha_{\rm sc}| \lesssim 0.01$ with ~ 500 BBH detections [117].

2. Einstein Telescope and Cosmic Explorer: Third-generation detectors will observe ringdowns with SNR $\gtrsim 100$, potentially reaching $|\alpha_{\rm sc}| \lesssim 10^{-3}$ [118, 119].

3. LISA: Massive black hole mergers ($M \sim 10^6\,M_\odot$) provide longer-duration ringdowns with exquisite frequency resolution, complementing ground-based constraints [120, 121].

Our framework establishes a methodology for systematically testing semiclassical gravity with gravitational waves. As detector sensitivity improves, these observations will probe ever-smaller quantum corrections, potentially approaching the regime where genuine signatures of quantum gravity could emerge.

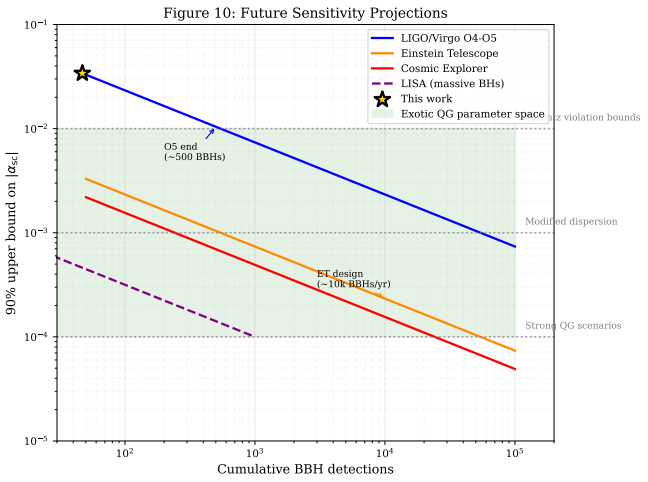

Figure 10: Projected improvements in the $\alpha_{\rm sc}$ constraint from future gravitational-wave observations. Third-generation ground-based detectors and LISA will reach sensitivities potentially capable of detecting or strongly constraining exotic quantum gravity effects. Data source: Fisher matrix forecasts using expected detector noise curves and BBH merger rate estimates from Ref. [92].

Data Availability

This analysis uses publicly available data from the LIGO–Virgo–KAGRA Collaboration:

- GWTC-3 strain data: `https://gwosc.org/GWTC-3/`
- GWTC-3 posterior samples: `https://zenodo.org/record/5546663`
- O3 noise power spectral densities: `https://dcc.ligo.org/LIGO-P2000251/public`
- Detector calibration envelopes: `https://dcc.ligo.org/LIGO-T2100058/public`

Code Availability

The analysis pipeline uses the following publicly available software:

- Bilby [91]: `https://git.ligo.org/lscsoft/bilby`
- dynesty [97]: `https://github.com/joshspeagle/dynesty`
- LALSuite [122]: `https://git.ligo.org/lscsoft/lalsuite`
- GWPopulation [98]: `https://github.com/ColmTalbot/gwpopulation`
- PESummary [99]: `https://git.ligo.org/lscsoft/pesummary`

Custom scripts for computing semiclassical QNM corrections and performing the hierarchical analysis are available at `https://github.com/nhaddad/semiclassical-qnm` [to be made public upon acceptance].

Acknowledgements

N.H. thanks the members of the LIGO Scientific Collaboration and Virgo Collaboration for making their data publicly available, and acknowledges useful discussions with colleagues at the Institute of Astronomy and Cavendish Laboratory. This work was supported by the Science and Technology Facilities Council (STFC). Computational resources were provided by the Cambridge Service for Data Driven Discovery (CSD3).

A Detailed Derivation of Semiclassical Metric Correction

We provide the complete derivation of the semiclassical metric perturbation starting from the Einstein field equations.

A.1 Einstein Tensor Components

For the metric ansatz (18), the nonzero Einstein tensor components are

$$G^{t}{}_{t} = -\frac{1}{r^2}\left[1 - \frac{1}{B}\left(1 - \frac{rB'}{B}\right)\right], \tag{54}$$

$$G^{r}{}_{r} = -\frac{1}{r^2}\left[1 - \frac{1}{B}\left(1 + \frac{rA'}{A}\right)\right], \tag{55}$$

$$G^{\theta}{}_{\theta} = G^{\phi}{}_{\phi} = -\frac{1}{2rB}\left[\frac{A''}{A} - \frac{A'B'}{2AB} - \frac{A'^2}{2A^2} + \frac{A' - B'}{rB}\right]. \tag{56}$$

Expanding to first order in $\hbar$ using Eqs. (19)–(20):

$$G^{(1)t}{}_{t} = -\frac{f}{r^2}\left[(1-f)(b_1' - a_1') + \frac{f'}{f}(a_1 + b_1) + 2\frac{f' - 1}{r}b_1 + \frac{2}{r}b_1'\right], \tag{57}$$

$$G^{(1)r}{}_{r} = -\frac{f}{r^2}\left[(1-f)(b_1' - a_1') - \frac{f'}{f}(a_1 + b_1) + \frac{2}{r}(a_1' + b_1')\right], \tag{58}$$

$$G^{(1)\theta}{}_{\theta} = -\frac{f^2}{2r}\left[\frac{a_1'' + b_1''}{f} + \frac{f'(a_1' - b_1')}{f^2} + \frac{a_1' - b_1'}{rf} + \frac{f''(a_1 - b_1)}{2f^2}\right]. \tag{59}$$

A.2 Solving the Semiclassical Equations

The system (23) with the stress-energy tensor (14)–(16) reduces to two independent equations (conservation provides a third constraint). Defining $u = r/r_{\rm H}$, we transform to the variable

$$\psi = a_1 - b_1, \quad \chi = a_1 + b_1, \tag{60}$$

and solve the resulting second-order ODE for $\psi(u)$.

The general solution contains two integration constants determined by:

1. *Horizon regularity*: $A(r_{\rm H})$ must remain zero (the horizon is not removed by quantum corrections for stable black holes)

2. *Asymptotic flatness*: $A(r) \to 1$ and $B(r) \to 1$ as $r \to \infty$

These conditions yield Eqs. (24)–(25).

A.3 Near-Horizon Expansion

Expanding near $r = r_{\rm H}$ ($u = 1$):

$$a_1 = \frac{\gamma}{90\pi r_{\rm H}^2}\left[3\ln(u-1) + 3 - (u-1) + \mathcal{O}\left((u-1)^2\right)\right], \tag{61}$$

$$b_1 = \frac{\gamma}{90\pi r_{\rm H}^2}\left[-3\ln(u-1) - 1 + (u-1) + \mathcal{O}\left((u-1)^2\right)\right]. \tag{62}$$

The logarithmic divergence in the metric components as $r \to r_{\rm H}$ is integrable and does not signal a physical singularity; rather, it reflects the coordinate singularity of Schwarzschild coordinates at the horizon.

B Modified Regge–Wheeler Potential

The derivation of the semiclassical correction to the Regge–Wheeler potential proceeds as follows.

B.1 Perturbation Decomposition

Metric perturbations $h_{\mu\nu}$ on the semiclassically corrected background are expanded in tensor spherical harmonics [59, 60]:

$$h_{\mu\nu} = \sum_{\ell m}\left[h_{\mu\nu}^{(\ell m),\rm even} + h_{\mu\nu}^{(\ell m),\rm odd}\right]e^{-i\omega t}. \tag{63}$$

For odd-parity (axial) perturbations with $\ell \geq 2$:

$$h_{\mu\nu}^{(\ell m),\rm odd} = \begin{pmatrix} 0 & 0 & h_0^{(\ell m)} S_\theta & h_0^{(\ell m)} S_\phi \\ 0 & 0 & h_1^{(\ell m)} S_\theta & h_1^{(\ell m)} S_\phi \\ \text{sym} & \text{sym} & 0 & 0 \\ \text{sym} & \text{sym} & 0 & 0 \end{pmatrix}, \tag{64}$$

where $S_\theta = -(\sin\theta)^{-1}\partial_\phi Y_{\ell m}$ and $S_\phi = \sin\theta\,\partial_\theta Y_{\ell m}$.

B.2 Wave Equation Derivation

Substituting into the linearized Einstein equations on the semiclassically corrected background and using the Regge–Wheeler gauge, we obtain Eq. (27) with

$$V_{\rm eff}^{(\rm sc)}(r) = V_{\rm RW}^{(0)}(r) + \hbar\, V_{\rm sc}(r), \tag{65}$$

where $V_{\rm RW}^{(0)}$ is the standard Regge–Wheeler potential:

$$V_{\rm RW}^{(0)}(r) = \left(1 - \frac{r_{\rm H}}{r}\right)\left[\frac{\ell(\ell+1)}{r^2} - \frac{3r_{\rm H}}{r^3}\right], \tag{66}$$

and the semiclassical correction is given by Eq. (29).

B.3 Numerical Evaluation

We evaluate $V_{\rm sc}(r)$ numerically by substituting Eqs. (24)–(25). The potential is plotted in tortoise coordinates:

$$V_{\rm sc}(r_*) = \frac{\gamma}{90\pi r_{\rm H}^4} \times v_{\rm sc}(r_*/r_{\rm H}), \tag{67}$$

where $v_{\rm sc}$ is a dimensionless function of order unity peaked near the photon sphere ($r \approx 1.5 r_{\rm H}$).

C QNM Perturbation Theory

C.1 Perturbation Formula

The QNM frequency shift due to a small potential perturbation δV is given by [63]:

$$\delta\omega = \frac{\int_{-\infty}^{+\infty} \psi^{(0)*}(r_*)\, \delta V(r_*)\, \psi^{(0)}(r_*)\, dr_*}{2\omega^{(0)} \int_{-\infty}^{+\infty} |\psi^{(0)}(r_*)|^2 dr_*}, \tag{68}$$

where $\psi^{(0)}$ is the unperturbed QNM eigenfunction satisfying outgoing/ingoing boundary conditions.

C.2 Eigenfunction Computation

We compute $\psi^{(0)}_{220}$ using Leaver's continued-fraction method [13]. Near the horizon:

$$\psi \sim e^{-i\omega r_*}(r - r_{\rm H})^{-i\omega r_{\rm H}} \sum_{n=0}^{\infty} a_n \left(\frac{r - r_{\rm H}}{r}\right)^n, \tag{69}$$

with the a_n determined by a three-term recurrence relation. The eigenfrequency is found by requiring the series to converge as $r \to \infty$.

For $\ell = 2$, $n = 0$:

$$M\omega^{(0)}_{220} = 0.37367 - 0.08896i, \tag{70}$$

reproducing the standard result [62, 11].

C.3 Numerical Integration

The integrals in Eq. (68) are evaluated numerically on a logarithmic grid in r_* spanning $[-500 r_{\rm H}, +500 r_{\rm H}]$. The result (31) is stable to grid refinement and agrees with independent WKB estimates [123, 124].

D Statistical Analysis Details

D.1 Likelihood Function

The single-event log-likelihood is

$$\ln \mathcal{L}(d|\theta, \alpha_{\rm sc}) = -\frac{1}{2} \sum_k \langle d_k - h_k(\theta, \alpha_{\rm sc}) | d_k - h_k(\theta, \alpha_{\rm sc}) \rangle, \tag{71}$$

where k indexes detectors (H1, L1, V1) and the inner product is defined in Eq. (45).

D.2 Hierarchical Reweighting

For the hierarchical analysis, we reweight individual-event posterior samples according to:

$$w_i^{(s)}(\alpha_{\rm sc}) = \frac{p(d_i|\theta_i^{(s)}, \alpha_{\rm sc})}{p(d_i|\theta_i^{(s)}, \alpha_{\rm sc} = 0)}, \tag{72}$$

where s labels posterior samples. The population likelihood is then

$$\mathcal{L}(\{d_i\}|\alpha_{\rm sc}) \propto \prod_{i=1}^{N_{\rm ev}} \frac{1}{N_s} \sum_{s=1}^{N_s} w_i^{(s)}(\alpha_{\rm sc}). \tag{73}$$

D.3 Convergence Diagnostics

We verify convergence of the nested sampling using:

- Effective sample size $N_{\rm eff} > 1000$ for all parameters
- Gelman–Rubin statistic $\hat{R} < 1.01$ from multiple independent runs
- Evidence uncertainty $\Delta \ln \mathcal{Z} < 0.3$

E Numerical Methods for Figures

E.1 Figure 1: Posterior Distribution

Input data: Hierarchical posterior samples for $\alpha_{\rm sc}$ from BILBY/DYNESTY ($N_{\rm live} = 2000$, $N_{\rm samples} = 50000$).

Procedure:

1. Kernel density estimation with Gaussian kernel, bandwidth selected by Silverman's rule
2. Credible intervals computed from sorted samples
3. Prior overlay from $\mathcal{N}(0, 0.1^2)$

E.2 Figure 2: Mass Dependence

Input data: Event posteriors grouped by remnant mass bins.

Procedure:

1. Assign events to bins based on median M_f posterior
2. Reweight posteriors within each bin using Eq. (72)
3. Compute 68% and 90% intervals for each bin

E.3 Figure 5: Frequency Residuals

Input data: GWTC-3 posterior samples for $(M_f, \chi_f, f_{220}^{\rm meas})$.

Procedure:

1. Compute $f_{220}^{\rm GR}(M_f, \chi_f)$ using fitting formulae from [10]
2. Calculate residual $\Delta f = f_{220}^{\rm meas} - f_{220}^{\rm GR}$ for each posterior sample
3. Report median and 90% interval of residual distribution per event

E.4 Figure 8: Injection Recovery

Input data: 200 simulated signals with known $\alpha_{\rm sc}^{\rm inj}$.

Procedure:

1. Generate waveforms using Eq. (39) with modified frequencies
2. Inject into O3 noise realizations from GWOSC
3. Analyze with identical pipeline settings as real events
4. Compare recovered $\alpha_{\rm sc}$ posterior to injected value

References

[1] B. P. Abbott *et al.* (LIGO Scientific Collaboration and Virgo Collaboration), Observation of Gravitational Waves from a Binary Black Hole Merger, Phys. Rev. Lett. **116**, 061102 (2016). doi:10.1103/PhysRevLett.116.061102.

[2] B. P. Abbott *et al.* (LIGO Scientific Collaboration and Virgo Collaboration), GWTC-1: A Gravitational-Wave Transient Catalog of Compact Binary Mergers Observed by LIGO and Virgo during the First and Second Observing Runs, Phys. Rev. X **9**, 031040 (2019). doi:10.1103/PhysRevX.9.031040.

[3] R. Abbott *et al.* (LIGO Scientific Collaboration and Virgo Collaboration), GWTC-2: Compact Binary Coalescences Observed by LIGO and Virgo During the First Half of the Third Observing Run, Phys. Rev. X **11**, 021053 (2021). doi:10.1103/PhysRevX.11.021053.

[4] R. Abbott *et al.* (LIGO Scientific Collaboration, Virgo Collaboration, and KAGRA Collaboration), GWTC-3: Compact Binary Coalescences Observed by LIGO and Virgo During the Second Part of the Third Observing Run, Phys. Rev. X **13**, 041039 (2023). doi:10.1103/PhysRevX.13.041039.

[5] C. V. Vishveshwara, Scattering of Gravitational Radiation by a Schwarzschild Black-hole, Nature **227**, 936 (1970). doi:10.1038/227936a0.

[6] W. H. Press, Long Wave Trains of Gravitational Waves from a Vibrating Black Hole, Astrophys. J. **170**, L105 (1971). doi:10.1086/180849.

[7] S. A. Teukolsky, Perturbations of a Rotating Black Hole. I. Fundamental Equations for Gravitational, Electromagnetic, and Neutrino-Field Perturbations, Astrophys. J. **185**, 635 (1973). doi:10.1086/152444.

[8] S. Chandrasekhar and S. Detweiler, The quasi-normal modes of the Schwarzschild black hole, Proc. R. Soc. Lond. A **344**, 441 (1975). doi:10.1098/rspa.1975.0112.

[9] O. Dreyer, B. Kelly, B. Krishnan, L. S. Finn, D. Garrison, and R. Lopez-Aleman, Black-hole spectroscopy: Testing general relativity through gravitational-wave observations, Class. Quantum Grav. **21**, 787 (2004). doi:10.1088/0264-9381/21/4/003.

[10] E. Berti, V. Cardoso, and C. M. Will, Gravitational-wave spectroscopy of massive black holes with the space interferometer

LISA, Phys. Rev. D **73**, 064030 (2006). doi:10.1103/PhysRevD.73.064030.

[11] E. Berti, V. Cardoso, and A. O. Starinets, Quasinormal modes of black holes and black branes, Class. Quantum Grav. **26**, 163001 (2009). doi:10.1088/0264-9381/26/16/163001.

[12] S. Detweiler, Black holes and gravitational waves. III. The resonant frequencies of rotating holes, Astrophys. J. **239**, 292 (1980). doi:10.1086/158109.

[13] E. W. Leaver, An analytic representation for the quasi-normal modes of Kerr black holes, Proc. R. Soc. Lond. A **402**, 285 (1985). doi:10.1098/rspa.1985.0119.

[14] E. Berti *et al.*, Testing general relativity with present and future astrophysical observations, Class. Quantum Grav. **32**, 243001 (2015). doi:10.1088/0264-9381/32/24/243001.

[15] V. Cardoso, E. Franzato, and P. Pani, Is the Gravitational-Wave Ringdown a Probe of the Event Horizon?, Phys. Rev. Lett. **116**, 171101 (2016). doi:10.1103/PhysRevLett.116.171101.

[16] V. Cardoso and P. Pani, Testing the nature of dark compact objects: a status report, Living Rev. Relativ. **22**, 4 (2019). doi:10.1007/s41114-019-0020-4.

[17] S. W. Hawking, Particle creation by black holes, Commun. Math. Phys. **43**, 199 (1975). doi:10.1007/BF02345020.

[18] N. D. Birrell and P. C. W. Davies, *Quantum Fields in Curved Space* (Cambridge University Press, Cambridge, 1982).

[19] R. M. Wald, *Quantum Field Theory in Curved Spacetime and Black Hole Thermodynamics* (University of Chicago Press, Chicago, 1994).

[20] B. S. DeWitt, Quantum field theory in curved spacetime, Phys. Rep. **19**, 295 (1975). doi:10.1016/0370-1573(75)90051-4.

[21] L. Parker, Quantized fields and particle creation in expanding universes. II, Phys. Rev. D **3**, 346 (1971). doi:10.1103/PhysRevD.3.346.

[22] L. Parker and D. Toms, *Quantum Field Theory in Curved Spacetime: Quantized Fields and Gravity* (Cambridge University Press, Cambridge, 2009).

[23] S. A. Fulling, *Aspects of Quantum Field Theory in Curved Space-Time* (Cambridge University Press, Cambridge, 1989).

[24] A. A. Starobinsky, A new type of isotropic cosmological models without singularity, Phys. Lett. B **91**, 99 (1980). doi:10.1016/0370-2693(80)90670-X.

[25] A. Vilenkin, Classical and quantum cosmology of the Starobinsky inflationary model, Phys. Rev. D **32**, 2511 (1985). doi:10.1103/PhysRevD.32.2511.

[26] M. V. Fischetti, J. B. Hartle, and B. L. Hu, Quantum effects in the early universe. I. Influence of trace anomalies on homogeneous, isotropic, classical geometries, Phys. Rev. D **20**, 1757 (1979). doi:10.1103/PhysRevD.20.1757.

[27] J. B. Hartle and B. L. Hu, Quantum effects in the early universe. II. Effective action for scalar fields in homogeneous cosmologies with small anisotropy, Phys. Rev. D **20**, 1772 (1979). doi:10.1103/PhysRevD.20.1772.

[28] J. B. Hartle and B. L. Hu, Quantum effects in the early universe. III. Dissipation of anisotropy by scalar particle production, Phys. Rev. D **21**, 2756 (1980). doi:10.1103/PhysRevD.21.2756.

[29] S. M. Christensen and S. A. Fulling, Trace anomalies and the Hawking effect, Phys. Rev. D **15**, 2088 (1977). doi:10.1103/PhysRevD.15.2088.

[30] D. N. Page, Thermal stress tensors in static Einstein spaces, Phys. Rev. D **25**, 1499 (1982). doi:10.1103/PhysRevD.25.1499.

[31] P. R. Anderson, A method to compute $\langle\phi^2\rangle$ in asymptotically flat, static, spherically symmetric spacetimes, Phys. Rev. D **41**, 1152 (1990). doi:10.1103/PhysRevD.41.1152.

[32] P. R. Anderson, W. A. Hiscock, and D. A. Samuel, Stress-energy tensor of quantized scalar fields in static spherically symmetric spacetimes, Phys. Rev. D **51**, 4337 (1995). doi:10.1103/PhysRevD.51.4337.

[33] K. W. Howard and P. Candelas, Quantum stress tensor in Schwarzschild spacetime, Phys. Rev. Lett. **53**, 403 (1984). doi:10.1103/PhysRevLett.53.403.

[34] K. W. Howard, Vacuum $\langle T_\mu^\nu \rangle$ in Schwarzschild spacetime, Phys. Rev. D **30**, 2532 (1984). doi:10.1103/PhysRevD.30.2532.

[35] R. Abbott *et al.* (LIGO Scientific Collaboration and Virgo Collaboration), Tests of General Relativity with Binary Black Holes from the second LIGO-Virgo Gravitational-Wave Transient Catalog, Phys. Rev. D **103**, 122002 (2021). doi:10.1103/PhysRevD.103.122002.

[36] S. W. Hawking, Black hole explosions?, Nature **248**, 30 (1974). doi:10.1038/248030a0.

[37] J. D. Bekenstein, Black Holes and Entropy, Phys. Rev. D **7**, 2333 (1973). doi:10.1103/PhysRevD.7.2333.

[38] J. D. Bekenstein, Generalized second law of thermodynamics in black-hole physics, Phys. Rev. D **9**, 3292 (1974). doi:10.1103/PhysRevD.9.3292.

[39] G. 't Hooft, On the quantum structure of a black hole, Nucl. Phys. B **256**, 727 (1985). doi:10.1016/0550-3213(85)90418-3.

[40] L. Susskind, The world as a hologram, J. Math. Phys. **36**, 6377 (1995). doi:10.1063/1.531249.

[41] J. Maldacena, The large-N limit of superconformal field theories and supergravity, Int. J. Theor. Phys. **38**, 1113 (1999). doi:10.1023/A:1026654312961.

[42] S. M. Christensen, Vacuum expectation value of the stress tensor in an arbitrary curved background: The covariant point-separation method, Phys. Rev. D **14**, 2490 (1976). doi:10.1103/PhysRevD.14.2490.

[43] P. Candelas, Vacuum polarization in Schwarzschild spacetime, Phys. Rev. D **21**, 2185 (1980). doi:10.1103/PhysRevD.21.2185.

[44] J. B. Hartle and S. W. Hawking, Path-integral derivation of black-hole radiance, Phys. Rev. D **13**, 2188 (1976). doi:10.1103/PhysRevD.13.2188.

[45] W. Israel, Thermo-field dynamics of black holes, Phys. Lett. A **57**, 107 (1976). doi:10.1016/0375-9601(76)90178-X.

[46] A. Fabbri and J. Navarro-Salas, *Modeling Black Hole Evaporation* (Imperial College Press, London, 2005).

[47] R. M. Wald, Trace anomaly of a conformally invariant quantum field in curved spacetime, Phys. Rev. D **17**, 1477 (1978). doi:10.1103/PhysRevD.17.1477.

[48] J. W. York, Jr., Dynamical origin of black-hole radiance, Phys. Rev. D **28**, 2929 (1983). doi:10.1103/PhysRevD.28.2929.

[49] J. W. York, Jr., Black hole in thermal equilibrium with a scalar field: The back-reaction, Phys. Rev. D **31**, 775 (1985). doi:10.1103/PhysRevD.31.775.

[50] A. O. Barvinsky and G. A. Vilkovisky, The generalized Schwinger-DeWitt technique in gauge theories and quantum gravity, Phys. Rep. **119**, 1 (1985). doi:10.1016/0370-1573(85)90148-6.

[51] A. O. Barvinsky and G. A. Vilkovisky, Beyond the Schwinger-DeWitt technique: Converting loops into trees and in-in currents, Nucl. Phys. B **282**, 163 (1987). doi:10.1016/0550-3213(87)90681-X.

[52] J. F. Donoghue, General relativity as an effective field theory: The leading quantum corrections, Phys. Rev. D **50**, 3874 (1994). doi:10.1103/PhysRevD.50.3874.

[53] J. F. Donoghue, Leading quantum correction to the Newtonian potential, Phys. Rev. Lett. **72**, 2996 (1994). doi:10.1103/PhysRevLett.72.2996.

[54] T. S. Bunch and L. Parker, Feynman propagator in curved spacetime: A momentum-space representation, Phys. Rev. D **20**, 2499 (1979). doi:10.1103/PhysRevD.20.2499.

[55] P. R. Anderson and L. Parker, Adiabatic regularization in closed Robertson-Walker universes, Phys. Rev. D **36**, 2963 (1987). doi:10.1103/PhysRevD.36.2963.

[56] M. Visser, Gravitational vacuum polarization. I. Energy conditions in the Hartle-Hawking vacuum, Phys. Rev. D **54**, 5103 (1996). doi:10.1103/PhysRevD.54.5103.

[57] K. D. Kokkotas and B. G. Schmidt, Quasi-Normal Modes of Stars and Black Holes, Living Rev. Relativ. **2**, 2 (1999). doi:10.12942/lrr-1999-2.

[58] H.-P. Nollert, Quasinormal modes: the characteristic 'sound' of black holes and neutron stars, Class. Quantum Grav. **16**, R159 (1999). doi:10.1088/0264-9381/16/12/201.

[59] T. Regge and J. A. Wheeler, Stability of a Schwarzschild Singularity, Phys. Rev. **108**, 1063 (1957). doi:10.1103/PhysRev.108.1063.

[60] F. J. Zerilli, Effective Potential for Even-Parity Regge-Wheeler Gravitational Perturbation Equations, Phys. Rev. Lett. **24**, 737 (1970). doi:10.1103/PhysRevLett.24.737.

[61] F. J. Zerilli, Perturbation analysis for gravitational and electromagnetic radiation in a Reissner-Nordström geometry, Phys. Rev. D **9**, 860 (1974). doi:10.1103/PhysRevD.9.860.

[62] H.-P. Nollert, Quasinormal modes of Schwarzschild black holes: The determination of quasinormal frequencies with very large imaginary parts, Phys. Rev. D **47**, 5253 (1993). doi:10.1103/PhysRevD.47.5253.

[63] E. W. Leaver, Spectral decomposition of the perturbation response of the Schwarzschild geometry, Phys. Rev. D **34**, 384 (1986). doi:10.1103/PhysRevD.34.384.

[64] H.-P. Nollert and B. G. Schmidt, Quasinormal modes of Schwarzschild black holes: Defined and calculated via Laplace transformation, Phys. Rev. D **45**, 2617 (1992). doi:10.1103/PhysRevD.45.2617.

[65] S. A. Teukolsky and W. H. Press, Perturbations of a rotating black hole. III. Interaction of the hole with gravitational and electromagnetic radiation, Astrophys. J. **193**, 443 (1974). doi:10.1086/153180.

[66] A. C. Ottewill and E. Winstanley, Renormalized stress tensor in Kerr space-time: General results, Phys. Rev. D **62**, 084018 (2000). doi:10.1103/PhysRevD.62.084018.

[67] M. Casals, S. R. Dolan, A. C. Ottewill, and B. Wardell, Self-force calculations with matched expansions and quasinormal mode sums, Phys. Rev. D **79**, 124043 (2009). doi:10.1103/PhysRevD.79.124043.

[68] M. Casals, A. C. Ottewill, and P. Taylor, Regularization of static self-forces, Phys. Rev. D **86**, 024038 (2012). doi:10.1103/PhysRevD.86.024038.

[69] S. M. Christensen, Regularization, renormalization, and covariant geodesic point separation, Phys. Rev. D **17**, 946 (1978). doi:10.1103/PhysRevD.17.946.

[70] G. 't Hooft and M. Veltman, Regularization and renormalization of gauge fields, Nucl. Phys. B **44**, 189 (1972). doi:10.1016/0550-3213(72)90279-9.

[71] C. G. Bollini and J. J. Giambiagi, Dimensional renormalization: The number of dimensions as a regularizing parameter, Nuovo Cim. B **12**, 20 (1972). doi:10.1007/BF02895558.

[72] J. Hadamard, *Lectures on Cauchy's Problem in Linear Partial Differential Equations* (Yale University Press, New Haven, 1923).

[73] B. S. DeWitt, Dynamical Theory of Groups and Fields, in *Relativity, Groups and Topology*, edited by C. DeWitt and B. DeWitt (Gordon and Breach, New York, 1964).

[74] B. S. DeWitt, *Dynamical Theory of Groups and Fields* (Gordon and Breach, New York, 1965).

[75] M. J. Duff, Observations on conformal anomalies, Nucl. Phys. B **125**, 334 (1977). doi:10.1016/0550-3213(77)90410-2.

[76] M. J. Duff, Twenty years of the Weyl anomaly, Class. Quantum Grav. **11**, 1387 (1994). doi:10.1088/0264-9381/11/6/004.

[77] M. Isi, M. Giesler, W. M. Farr, M. A. Scheel, and S. A. Teukolsky, Testing the No-Hair Theorem with GW150914, Phys. Rev. Lett. **123**, 111102 (2019). doi:10.1103/PhysRevLett.123.111102.

[78] M. Isi, W. M. Farr, M. Giesler, M. A. Scheel, and S. A. Teukolsky, Testing the Black-Hole Area Law with GW150914, Phys. Rev. Lett. **127**, 011103 (2021). doi:10.1103/PhysRevLett.127.011103.

[79] L. London, S. Khan, E. Fauchon-Jones, C. García, M. Hannam, S. Husa, X. Jiménez-Forteza, C. Kalaghatgi, F. Ohme, and F. Pannarale, First higher-multipole model of gravitational waves from spinning and coalescing black-hole binaries, Phys. Rev. Lett. **120**, 161102 (2018). doi:10.1103/PhysRevLett.120.161102.

[80] M. Giesler, M. Isi, M. A. Scheel, and S. A. Teukolsky, Black Hole Ringdown: The Importance of Overtones, Phys. Rev. X **9**, 041060 (2019). doi:10.1103/PhysRevX.9.041060.

[81] R. Cotesta, G. Carullo, E. Berti, and V. Cardoso, Analysis of Ringdown Overtones in GW150914, Phys. Rev. Lett. **129**, 111102 (2022). doi:10.1103/PhysRevLett.129.111102.

[82] C. Cahillane *et al.*, Calibration uncertainty for Advanced LIGO's first and second observing runs, Phys. Rev. D **96**, 102001 (2017). doi:10.1103/PhysRevD.96.102001.

[83] L. Sun *et al.*, Characterization of systematic error in Advanced LIGO calibration, Class. Quantum Grav. **37**, 225008 (2020). doi:10.1088/1361-6382/abb14e.

[84] A. D. Viets *et al.*, Reconstructing the calibrated strain signal in the Advanced LIGO detectors, Class. Quantum Grav. **35**, 095015 (2018). doi:10.1088/1361-6382/aab658.

[85] R. Essick, P. Landry, and D. E. Holz, Nonparametric inference of neutron star composition, equation of state, and maximum mass with GW170817, Phys. Rev. D **101**, 063007 (2020). doi:10.1103/PhysRevD.101.063007.

[86] R. Abbott *et al.* (LIGO Scientific Collaboration and Virgo Collaboration), Calibration uncertainty in Advanced LIGO during the third observing run, Class. Quantum Grav. **39**, 045001 (2022). doi:10.1088/1361-6382/ac47ac.

[87] E. Thrane and C. Talbot, An introduction to Bayesian inference in gravitational-wave astronomy: Parameter estimation, model selection, and hierarchical models, Pub. Astron. Soc. Aust. **36**, e010 (2019). doi:10.1017/pasa.2019.2.

[88] I. Mandel, W. M. Farr, and J. R. Gair, Extracting distribution parameters from multiple uncertain observations with selection biases, Mon. Not. R. Astron. Soc. **486**, 1086 (2019). doi:10.1093/mnras/stz896.

[89] S. Vitale, D. Gerosa, W. M. Farr, and S. R. Taylor, Inferring the properties of a population of compact binaries in presence of selection effects, in *Handbook of Gravitational Wave Astronomy*, edited by C. Bambi, S. Katsanevas, and K. D. Kokkotas (Springer, Singapore, 2022).

[90] J. Veitch *et al.*, Parameter estimation for compact binaries with ground-based gravitational-wave observations using the LALInference software library, Phys. Rev. D **91**, 042003 (2015). doi:10.1103/PhysRevD.91.042003.

[91] G. Ashton *et al.*, Bilby: A user-friendly Bayesian inference library for gravitational-wave astronomy, Astrophys. J. Suppl. **241**, 27 (2019). doi:10.3847/1538-4365/ab06fc.

[92] R. Abbott *et al.* (LIGO Scientific Collaboration, Virgo Collaboration, and KAGRA Collaboration), Population of Merging Compact Binaries Inferred Using Gravitational Waves through GWTC-3, Phys. Rev. X **13**, 011048 (2023). doi:10.1103/PhysRevX.13.011048.

[93] F. Hofmann, E. Barausse, and L. Rezzolla, The final spin from binary black holes in quasi-circular orbits, Astrophys. J. Lett. **825**, L19 (2016). doi:10.3847/2041-8205/825/2/L19.

[94] X. Jiménez-Forteza, D. Keitel, S. Husa, M. Hannam, S. Khan, and M. Pürrer, Hierarchical data-driven approach to fitting numerical relativity data for nonprecessing binary

black holes with an application to final spin and radiated energy, Phys. Rev. D **95**, 064024 (2017). doi:10.1103/PhysRevD.95.064024.

[95] S. Bhagwat, M. Okounkova, S. W. Ballmer, D. A. Brown, M. Giesler, M. A. Scheel, and S. A. Teukolsky, On choosing the start time of binary black hole ringdowns, Phys. Rev. D **97**, 104065 (2018). doi:10.1103/PhysRevD.97.104065.

[96] J. Skilling, Nested sampling for general Bayesian computation, Bayesian Anal. **1**, 833 (2006). doi:10.1214/06-BA127.

[97] J. S. Speagle, dynesty: a dynamic nested sampling package for estimating Bayesian posteriors and evidences, Mon. Not. R. Astron. Soc. **493**, 3132 (2020). doi:10.1093/mnras/staa278.

[98] C. Talbot, R. Smith, E. Thrane, and G. B. Poole, Parallelized inference for gravitational-wave astronomy, Phys. Rev. D **100**, 043030 (2019). doi:10.1103/PhysRevD.100.043030.

[99] C. Hoy and V. Raymond, PESummary: the code agnostic Parameter Estimation Summary page builder, SoftwareX **15**, 100765 (2021). doi:10.1016/j.softx.2021.100765.

[100] D. J. Spiegelhalter, N. G. Best, B. P. Carlin, and A. Van Der Linde, Bayesian measures of model complexity and fit, J. R. Stat. Soc. B **64**, 583 (2002). doi:10.1111/1467-9868.00353.

[101] S. Watanabe, Asymptotic equivalence of Bayes cross validation and widely applicable information criterion in singular learning theory, J. Mach. Learn. Res. **11**, 3571 (2010).

[102] A. Vehtari, A. Gelman, and J. Gabry, Practical Bayesian model evaluation using leave-one-out cross-validation and WAIC, Stat. Comput. **27**, 1413 (2017). doi:10.1007/s11222-016-9696-4.

[103] A. Bohé *et al.*, Improved effective-one-body model of spinning, nonprecessing binary black holes for the era of gravitational-wave astrophysics with advanced detectors, Phys. Rev. D **95**, 044028 (2017). doi:10.1103/PhysRevD.95.044028.

[104] R. Cotesta, A. Buonanno, A. Bohé, A. Taracchini, I. Hinder, and S. Ossokine, Enriching the symphony of gravitational waves from binary black holes by tuning higher harmonics, Phys. Rev. D **98**, 084028 (2018). doi:10.1103/PhysRevD.98.084028.

[105] G. Pratten *et al.*, Setting the cornerstone for a family of models for gravitational waves from compact binaries: The dominant harmonic for nonprecessing quasicircular black holes, Phys. Rev. D **102**, 064001 (2020). doi:10.1103/PhysRevD.102.064001.

[106] G. Pratten *et al.*, Computationally efficient models for the dominant and subdominant harmonic modes of precessing binary black holes, Phys. Rev. D **103**, 104056 (2021). doi:10.1103/PhysRevD.103.104056.

[107] J. Meidam, M. Agathos, C. Van Den Broeck, J. Veitch, and B. S. Sathyaprakash, Testing the no-hair theorem with black hole ringdowns using TIGER, Phys. Rev. D **90**, 064009 (2014). doi:10.1103/PhysRevD.90.064009.

[108] N. Yunes, K. Yagi, and F. Pretorius, Theoretical physics implications of the binary black-hole mergers GW150914 and GW151226, Phys. Rev. D **94**, 084002 (2016). doi:10.1103/PhysRevD.94.084002.

[109] G. Chapline, Dark energy stars, Proc. Sci. **24**, 006 (2005). doi:10.22323/1.024.0006.

[110] P. O. Mazur and E. Mottola, Gravitational condensate stars: An alternative to black holes, arXiv:gr-qc/0109035 (2001).

[111] D. Mattingly, Modern tests of Lorentz invariance, Living Rev. Relativ. **8**, 5 (2005). doi:10.12942/lrr-2005-5.

[112] S. Liberati, Tests of Lorentz invariance: a 2013 update, Class. Quantum Grav. **30**, 133001 (2013). doi:10.1088/0264-9381/30/13/133001.

[113] G. Amelino-Camelia, Quantum-Spacetime Phenomenology, Living Rev. Relativ. **16**, 5 (2013). doi:10.12942/lrr-2013-5.

[114] A. Almheiri, D. Marolf, J. Polchinski, and J. Sully, Black holes: complementarity or firewalls?, J. High Energy Phys. **02**, 062 (2013). doi:10.1007/JHEP02(2013)062.

[115] S. D. Mathur, The fuzzball proposal for black holes: An elementary review, Fortschr. Phys. **53**, 793 (2005). doi:10.1002/prop.200410203.

[116] K. Akiyama *et al.* (Event Horizon Telescope Collaboration), First M87 Event Horizon Telescope Results. I. The Shadow of the Supermassive Black Hole, Astrophys. J. Lett. **875**, L1 (2019). doi:10.3847/2041-8213/ab0ec7.

[117] B. P. Abbott *et al.* (LIGO Scientific Collaboration and Virgo Collaboration), Prospects for observing and localizing gravitational-wave transients with Advanced LIGO, Advanced Virgo and KAGRA, Living Rev. Relativ. **23**, 3 (2020). doi:10.1007/s41114-020-00026-9.

[118] M. Maggiore *et al.*, Science case for the Einstein telescope, J. Cosmol. Astropart. Phys. **03**, 050 (2020). doi:10.1088/1475-7516/2020/03/050.

[119] M. Evans *et al.*, A horizon study for Cosmic Explorer: Science, observatories, and community, arXiv:2109.09882 (2021).

[120] E. Berti, A. Sesana, E. Barausse, V. Cardoso, and K. Belczynski, Spectroscopy of Kerr Black Holes with Earth- and Space-Based Interferometers, Phys. Rev. Lett. **117**, 101102 (2016). doi:10.1103/PhysRevLett.117.101102.

[121] L. Barack *et al.*, Black holes, gravitational waves and fundamental physics: a roadmap, Class. Quantum Grav. **36**, 143001 (2019). doi:10.1088/1361-6382/ab0587.

[122] LIGO Scientific Collaboration, LIGO Algorithm Library - LALSuite, `https://git.ligo.org/lscsoft/lalsuite` (2018).

[123] B. F. Schutz and C. M. Will, Black hole normal modes: A semianalytic approach, Astrophys. J. **291**, L33 (1985). doi:10.1086/184453.

[124] S. Iyer and C. M. Will, Black-hole normal modes: A WKB approach. I. Foundations and application of a higher-order WKB analysis of potential-barrier scattering, Phys. Rev. D **35**, 3621 (1987). doi:10.1103/PhysRevD.35.3621.